Methods and Applications in Fluorescence

RECEIVED
31 October 2016

REVISED
10 April 2017

ACCEPTED FOR PUBLICATION
24 April 2017

PUBLISHED
15 May 2017

PAPER

Temperature dependent spectroscopic and excited state dynamics of 3-hydroxychromones with electron donor and acceptor substituents

Alan Szalai[1,2], Luciana Giordano[1,3], Verónica M Sánchez[2,4], Teresa D Z Atvars[5], Marcelo Faleiros[5], Elizabeth Jares-Erijman[3,6,7] and Pedro F Aramendía[1,2,8]

[1] Centro de Investigaciones en Bionanociencias 'Elizabeth Jares-Erijman' CIBION. CONICET. Godoy Cruz 2390. 1425 Ciudad de Buenos Aires. Argentina
[2] Departamento de Química Inorgánica, Analítica y Química Física. FCEN. UBA. Pabellón 2. Ciudad Universitaria. 1428 Ciudad de Buenos Aires. Argentina
[3] Departamento de Química Orgánica. FCEN. UBA. Pabellón 2. Ciudad Universitaria. 1428 Ciudad de Buenos Aires. Argentina
[4] Centro de Simulación Computacional para Aplicaciones Tecnológicas. CSC-CONICET. Godoy Cruz 2390. 1425 Ciudad de Buenos Aires. Argentina
[5] Chemistry Institute, University of Campinas. PO Box 6154. Campinas, SP, Brazil
[6] CIHIDECAR-CONICET. Pabellón 2. Ciudad Universitaria. 1428 Ciudad de Buenos Aires. Argentina
[7] Deceased September 29, 2011.
[8] Authors to whom any correspondence should be addressed.

E-mail: pedro.aramendia@cibion.conicet.gov.ar

Keywords: ratiometric probe, ESIPT, time resolved emission spectroscopy, anisotropy, TDDFT, fluorescence

Supplementary material for this article is available online

Abstract

We have studied the photophysical and photochemical behavior of three compounds derived from 3-hydroxychromone (3-HC), capable of undergoing excited state proton transfer (ESIPT). The compounds have two substituents, located in positions 2 and 7, one on each ring of the 3-HC heterocycle. The substituent pattern shows different electron donating and acceptor features. The compounds were studied by absorption and emission spectroscopy, steady state anisotropy, and time resolved emission spectroscopy (TRES) as a function of temperature. Results were interpreted using time dependent density functional theory calculations. Compared to reference compounds of 3-HC substituted only in the 2 position, the compounds show similar absorption and emission spectra, shifted 20–30 nm to higher wavelengths due to extended conjugation. TRES shows the existence of ESIPT in the thermodynamic equilibrium regime. This process is endothermic in all three compounds. The different behavior compared to monosubstituted 3-HC is attributed to the extended conjugation and to the electron donor acceptor character of the substituents, which has a more pronounced effect when the electron acceptor is located in position 2.

1. Introduction

Compounds that display intramolecular proton transfer find extensive applications in sensing [1–4] and in electro optical devices [5]. Among them, 3-hydroxychromone (3-HC) is the basic structure of a prominent family that displays a fluorescence originating from two different excited state tautomers, interconverted by an intramolecular proton transfer that takes place in the excited state. This process denoted from excited state intramolecular proton transfer (ESIPT) has attracted intense attention since the pioneering work of Kasha [6]. The emission properties and the dynamics of the ESIPT have been extensively studied by Demchenko and coworkers and recently reviewed [1, 7, 8]. The emission exhibits two bands; the one with the smaller Stokes shift originates from the normal excited state form, N^*, while a red shifted emission comes from the tautomer excited state, T^*, produced by ESIPT. This dual band emission is fundamental for the application of ESIPT compounds for sensing and optoelectronics.

Two extreme kinetic scenarios can be envisioned for the ESIPT process: (1) equilibration of N^* and T^* in

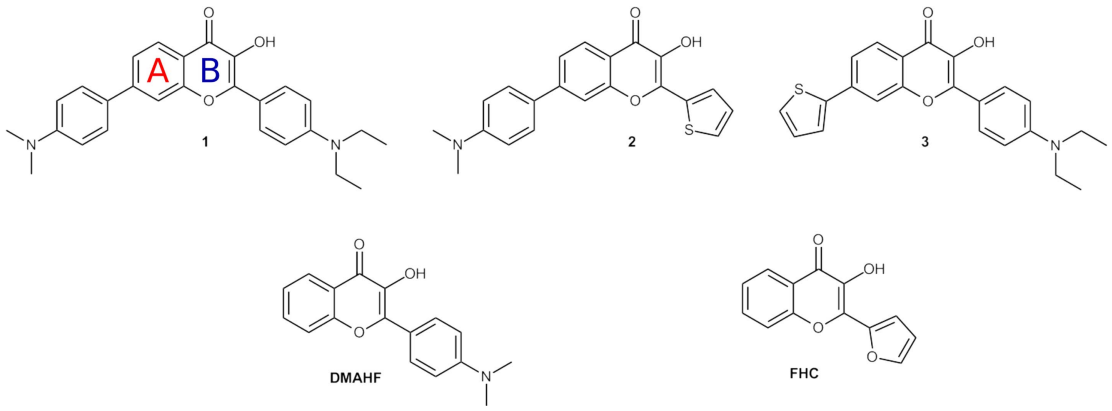

Scheme 1. Molecular structure of the ESIPT compounds **1–3** studied in this work and of DMAHF and FHC.

the excited state takes place much faster than deactivation of either state (thermodynamic control); and (2) lack of a reverse reaction of T^* to N^* during the excited state lifetime (kinetic control). These two extreme conditions exhibit distinctive, characteristic kinetic behaviors of the excited states and are thus easily distinguishable. Intermediate cases are also feasible, in which equilibration in the excited state and excited state decay take place with comparable rates. A key feature of ESIPT is the solvent dependence of the rate and extent of tautomerism. This medium sensitivity is the basis for applications of 3-HC as ratiometric probes.

A 3-HC that has been studied in great detail is 2-phenyl-3-HC, generally known as 3-hydroxyflavone (3-HF) [9–12]. In the case of 4-*N*,*N*-dimethylamino-3-HF (DMAHF), extensive time resolved emission studies [10, 13, 14] and structural calculations of the ground and excited state [15, 16] have been carried out. Upon excitation to the N^* state, there is a partial charge transfer from the dialkylamino group (which gains positive charge density) to the carbonyl oxygen (which gains negative charge density), remaining the charge density on the hydroxyl oxygen practically unchanged. The tautomerization is accompanied by an exchange in the values of the charge density of the two oxygen atoms. The ground state of this compound is exclusively in the *N* tautomer form [16].

Substitution in 3-HC derivatives have been mainly performed on position 2 of ring B (scheme 1) and lead to modulation of the dynamics and the equilibrium position of the two tautomers in the excited state [17]. Studies of the excited state dynamics of this family of B ring substituted flavones in the femto to nanosecond timescale [9, 18, 19] indicate that the compound is present in its *N* form in the ground state and T^* emission originates after ESIPT. In these time resolved emission experiments no emission from T^* immediately after excitation at ~400 nm was observed and T^* built up from the initially excited N^*.

Modification of ring A has been more rarely performed. For example, a dialkylaminophenyl group in position 7 of 3-HC enhances the solvatochromic sensitivity and emission quantum yield, while the ESIPT is almost completely inhibited in most solvents [20]. The addition of a methoxy moiety in position 7 has an influence on steady state spectra [17, 21] but other features of the emission have not been studied in depth. The spectroscopic features of two derivatives of 3-HC with substitution in position 2 and 7 were reported [22]. Compared to parent compounds lacking the substituent in position 7, the compounds show a red shifted absorption and emission, as well as enhanced solvatochromism and contribution from N^* emission. Another study reported that in 7-substituted DMAHF the emission quantum yield is enhanced in most solvents compared to the parent DMAHF, while the change from an electron acceptor isothiocyanate group to and electron donor thiourea, greatly enhances T^* emission [23]. Finally, an extended group of 2-aryl-7-aryl-3-HC compounds were synthesized and spectroscopically analyzed to ascertain the influence of substituents in the spectroscopic and solvatochromic features as well as in their binding to serum albumin [24].

In the present communication, we report the temperature dependent spectroscopy and excited state dynamics of three compounds derived from DMAHF (**1–3**, scheme 1). The presence of two substituents with different electron donor and acceptor properties in the basic 3-HC structure influences the ESIPT process as well as the solvatochromic sensitivity. Compound **1** has an electron donating substituent on ring A. Compound **2** has a mild electron withdrawing group on ring B and an electron donating moiety on ring A. The location of these groups is exchanged in compound **3**. We analyzed the spectroscopical features and excited state dynamics of **1–3** as a function of temperature. Our aim was to establish the activation and enthalpy differences of the two tautomers in the excited state, so as to explain the different behavior observed for the compounds and to gain insight in the influence of substituents on the environment sensing capacity. Studies were carried out by steady state fluorescence emission and excitation spectroscopy and anisotropy,

as well as by fluorescence decay and time-resolved emission spectroscopy. Results were interpreted with the help of TDDFT calculations.

2. Materials and methods

2.1. Chemicals

Fluorescent compounds **1–3** were synthesized starting from 3-bromophenol in four steps (details are given in the supporting information, SI is available online at stacks.iop.org/MAF/5/024011/mmedia). A brief description is given in what follows. The first step, common to all synthetic routes was the transformation of 3-bromophenol to 4′-bromo-2′-hydroxyacetophenone (**4**) with acyl chloride, using $AlCl_3$ in 1,2-dichloroethane via a Freis rearrangement [25]. Acetophenone **4** was condensed with 4-(diethylamino)benzaldehyde to yield 3-HC (**5**) in two steps applying a Algar–Flynn–Oyamada (AFO) method [26]. This compound was either set to react with 4-(dimethylamino)phenylboronic acid to yield compound **1**, or with 2-thiophenylboronic acid to render compound **3** via a Suzuki coupling reaction. To synthesize compound **2**, the order of the two key reactions, AFO and Suzuki coupling was reverted. **4** was first reacted with 4-(dimethylamino) phenylboronic acid and afterwards condensed with thiophene-2-carbaldehyde.

For spectroscopic measurements, all solvents, acetonitrile (Optima LC/MS, from Fisher Chemical), dichloromethane (DCM, Optima, from Fisher Chemical), *n*-octanol (99%, from Sigma), and toluene (Uvasol, from Merck) were used as received.

2.2. Absorption and emission steady state spectroscopy

Absorption spectra were recorded on a Shimadzu UV-3600 spectrophotometer, and fluorescence emission and excitation spectra were measured on a PTI QM40 spectrofluorometer. For measurements near room temperature, the sample was contained in a 1 cm square quartz cuvette with a teflon stopper and thermal control was achieved with a Peltier system. In the case of compound **2** in DCM a broader temperature range was used. In this case, the sample was contained in a sealed quartz tube. The sample was frozen with liquid nitrogen during tube sealing. For compound **2** in DCM, the sealed quartz tube was temperature controlled by a helium closed-cycle cryostat (APD Cryogenics D204) with a digital temperature controller model 9650 operating in a temperature range of −100 °C to 55 °C. All spectra were corrected for the intensity and sensitivity of the excitation and emission channels. Steady state anisotropy was measured in *n*-octanol as a function of the excitation or emission wavelength on the PTI fluorometer identified above. Polymer sheet polarizers were used in the excitation and in the emission channel. The *G* factor, correcting for the different sensitivity of the emission channel to vertical and horizontal polarization of light, was determined *in situ* using the same fluorescent solution.

2.3. Time dependent emission

Decay curves were recorded on a IBH-Horiba-Jovin-Ivon Time Correlated Single Photon Counting equipment. The sample was excited by a 1 MHz repetition rate LED (Horiba Jovin Ivon 405 nm LED, <100 ps FWHM pulse). Light passed through a monochromator before impinging on the sample in a 1 cm square quartz cuvette in a holder with circulating water. Using vertically polarized light, emission was recorded at the magic angle by a red enhanced PMT after passing through an emission monochromator. Decay curves were recorded at single emission wavelength until a maximal of 5000–10 000 counts were accumulated at the maximum. The counting rate was reduced to prevent photon pile up. A 50 ns time conversion range, distributed in 8192 channels (6.86 ps/channel), was chosen for all measurements. Mono- and bi-exponential fits were performed using the deconvolution software IBH-Data Station. For the extended temperature range utilized for compound **2** in DCM, the sample was measured on a single photon counting Edinburg Analytical Instruments FL900 with a MCP-PMT (Hamamatsu R3809U-50) detector using the same temperature regulating system as described above for this sample. Excitation was performed with a pulsed Picoquant LDH-D-C-405 diode laser (emission 405 nm, FWHM ∼150 ps). Other measurement conditions were kept similar. Time resolved emission spectra (TRES) were reconstructed by recording fluorescence decay curves between 460 and 660 nm, every 10 nm, at a fixed temperature. The time decays at each wavelength were corrected to reproduce the steady state spectra when integrated and emission spectra were reconstructed at different time points.

2.4. Quantum mechanical calculations

Calculations were performed using the Gaussian 09 program [27]. Geometry optimizations were calculated using DFT, in combination with CAM-B3LYP [28] hybrid functional and polarized valence triple-ζ basis set (TZVP), in accordance with previous reports [29]. *N* and *T* conformers of compounds **1–3** were optimized in presence of continuum solvent employing polarized continuum model (PCM) [30, 31] for DCM. HOMO and LUMO molecular orbitals displayed here were considered up to 0.04 e $bohr^{-3}$ isosurface density. HOMO-LUMO orbitals as well as charge transfer during the absorption processes are in line with the reported values for DMAF and FHC compounds [16]. See SI for details. Absorption energies were determined using TDDFT in combination with external iteration [32] -PCM to consider the

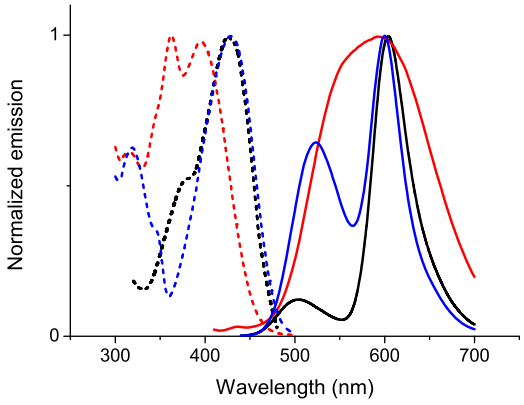

Figure 1. Steady state fluorescence excitation (dashed lines) and emission (solid lines) spectra of **1**–**3** in DCM at 15 °C. All spectra were normalized to the maximum and corrected for the wavelength sensitivity of the excitation and emission channels. **1** (black line) emission $\lambda_{exc} = 425$ nm; excitation $\lambda_{em} = 610$ nm; **2**: (red line) emission $\lambda_{exc} = 400$ nm; excitation $\lambda_{em} = 600$ nm; **3** (blue line) emission $\lambda_{exc} = 430$ nm; excitation $\lambda_{em} = 600$ nm.

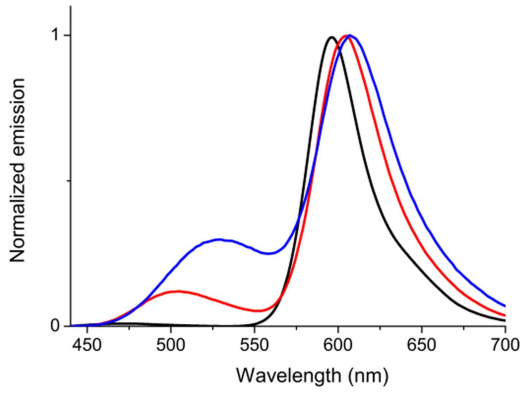

Figure 2. Steady state emission of **1** in ACN (blue), DCM (red), toluene (black).

solvent environment on the transition. Transition dipole moments were also obtained.

3. Results

Figure 1 displays the fluorescence emission and excitation spectra of **1**–**3** in DCM. The typical dual band ESIPT fluorescence emission was observed. To determine the position of the N^* and T^* emission maxima, Gaussian deconvolution of the spectra was performed on the wavenumber scale. The emission spectra of **1** and **3** needed to be deconvoluted to a sum of three Gaussian components, to achieve a better than 1% maximum deviation accuracy. From these Gaussian peaks, the two most to the red correspond to the T^* emission, and the one at the highest energy is ascribed to the N^* emission. The emission of **2** in DCM was adequately described with two Gaussian components. In this case the N^* and T^* bands had comparable amplitudes and were less resolved. For the sake of simplicity, we adopted the description with two components, corresponding to N^* (higher energy) and to T^* (lower energy). In other solvents and for the 3 compounds, a three Gaussian component deconvolution was adopted. In the SI we show examples of these fits for compounds **2** and **3**. The position of the maximum of each Gaussian peak, on the energy scale and the integrated area of the peaks were used to determine the thermochromic and solvatochromic shifts, as well as the integrated emission intensity ratio of N^* and T^*: I_{N^*}/I_{T^*} (see below).

The compounds studied in this work display a positive solvatochromism, as also does DMAHF, 7-aryl-3-HC and a whole family of 2,7-3-HC [20, 24]. As an example, the emission spectra of **1** in acetonitrile, DCM, and toluene are shown on figure 2. Like for 3-HC derivatives, the solvatochromic sensitivity is greater for the N^* band than for the T^* band [1].

The spectral distribution of absorption appears to be governed by the nature of the substituent on ring B. Under this assumption, we can justify the similarity between the excitation spectra of compounds **1** and **3**, and the similarity of the excitation spectrum of **2** with 2-(2-furyl)-3-hydroxychromone (FHC) [17]. The spectra of **1**–**3**, compared to DMAHF or FHC were shifted to the red by 20–30 nm due to extended conjugation. Compared to a closer analogue, 3-hydroxy-2-(thiophen-2-yl)-chromen-4-one (THC), the absorption of compound **2** is red shifted by 50 nm [33]. In contrast, the addition of a methoxy substituent on ring A lowers the contribution of N^* in the emission spectrum, compared to DMAHF [17].The emission spectrum of **1** displays the same difference (compared to **3**) that appears between DMAHF and its derivative with a methoxy substituent on ring A. Furthermore, the presence of a mild electron acceptor substituent on ring B has a profound influence on the emission spectral distribution of **2**. Its N^* originated emission is enhanced and red shifted compared to **1** and **3** and also shows the greatest temperature dependence of the emission energy (see below). Compared to the similar 7-aryl-3HC, without substituent on ring B, **2** shows ESIPT and an emission spectrum shifted to the red by more than 50 nm in DCM, from 503 nm for FHC [20] to 556 nm for **2** at 25 °C. This shift is much greater compared to 399 nm emission maximum of N^* for THC in acetone [31].

Figure 3 shows the temperature dependence of the emission spectra, and table 1 summarizes the position of the maximum of the spectral components as a function of temperature in ACN, DCM, and toluene. All display a blue shift of emission upon temperature increase. We attribute this behavior to a greater interaction with the environment of the excited state compared to the ground state [34]. The variation is greater for N^* than for T^*, in agreement with the higher solvatochromic shift reported for the N^* band for 3-HC and derivatives [1]. The ratio of total emission intensity of

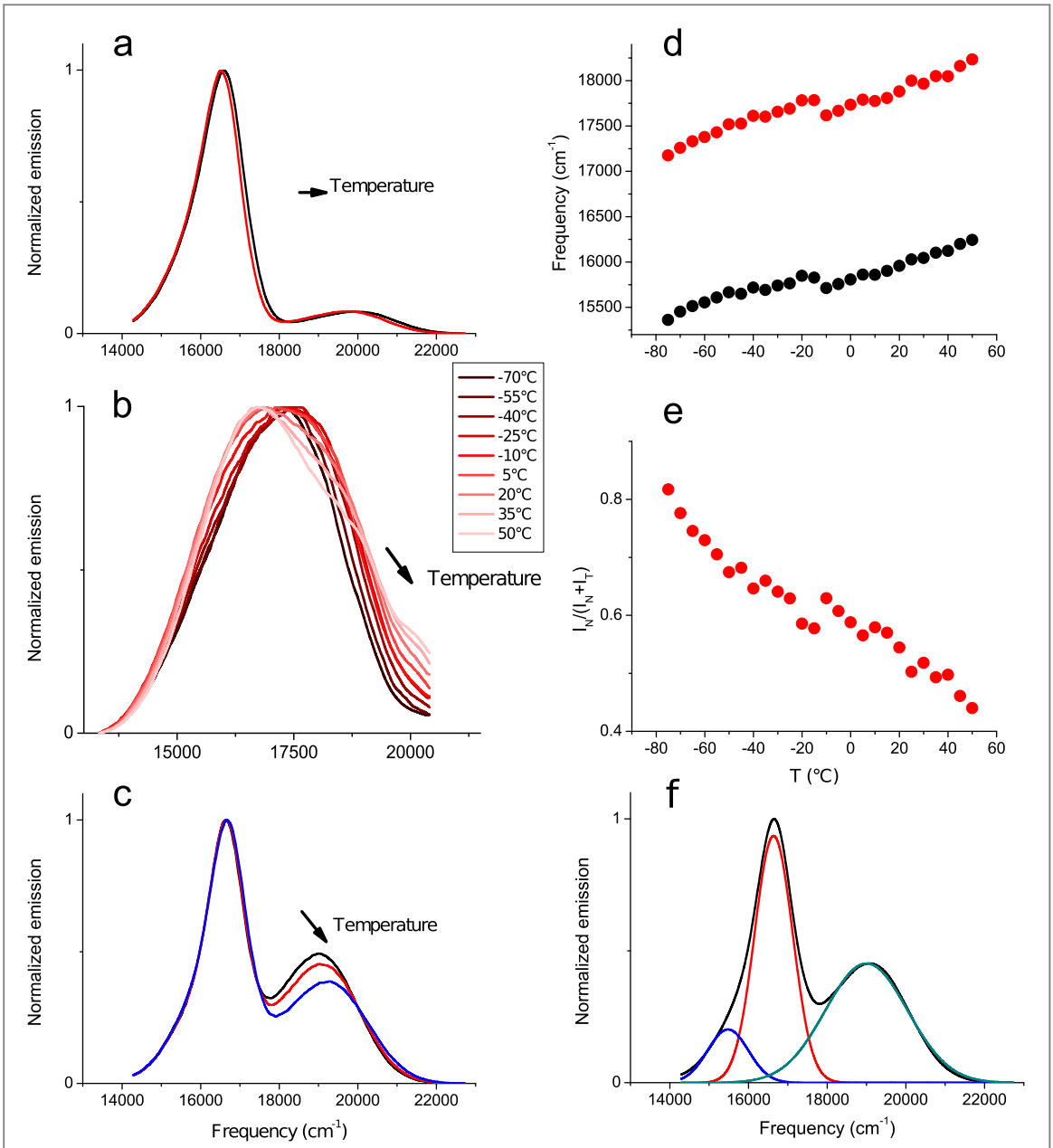

Figure 3. Emission spectra of **1**–**3** (panels (a)–(c), respectively) in DCM, normalized to the maximum, as a function of temperature. Temperature varies from 15 °C to 45 °C for **1** and **3**, and from −70 °C to 50 °C for **2**. The arrows indicate the direction of the change upon temperature increase. Panel (d): energy of the emission maximum of N^* (red dots) and T^* (black dots) of **2** obtained from the two component Gaussian deconvolution of the emission spectra of panel b (see text). Panel (e): fraction of N^* emission for **2** as a function of temperature, obtained from the integration of the deconvoluted spectra of panel b. Panel (f): spectral deconvolution into three Gaussian components of the emission spectrum of **3** in DCM at 25 °C.

N^* to T^*, I_{N^*}/I_{T^*}, was evaluated from the integral of the corresponding Gaussian components of the spectral deconvolution. Although this ratio shows no variation with temperature for **1** in DCM, it decreases with temperature increase for **2** and **3**, indicating a higher participation of T^* in the emission at higher temperatures. The emission spectra, normalized to the maximum, in DCM of **1**–**3**, as well as the temperature dependent emission fraction of N^*, $I_{N^*}/(I_{N^*} + I_{T^*})$, and the position of N^* and T^* emission for compound **2** are shown in figure 3.

Steady state anisotropy of excitation and emission were measured in *n*-octanol at 15 °C for **3** (figure 4). The excitation anisotropy spectrum shows the presence of at least two transitions with two distinct orientations of transition moments. The band at shorter wavelengths, between 300 and 370 nm, with a slightly negative anisotropy value may be associated to an excitation from ground state to an S_2 state, while the band at longer wavelengths, between 370 and 490 nm, can be attributed to excitation to the emissive S_1 excited state. The existence of these two absorption bands leading to two different excited states has recently been described in 3-HC derivatives that yield enhanced ESIPT when irradiated to higher excited states [35]. The steady state anisotropy value differs

Table 1. Wavelength of the maximum of each Gaussian component in the deconvolution of the emission spectra of **1**–**3** in ACN, DCM, and toluene as a function of temperature.

	15 °C			45 °C		
	λ_{max} (nm)					
	ACN	DCM	Tol	ACN	DCM	Tol
1						
N^*	535	509	476	531	504	472
$T1^*$	609	603	596	606	600	593
$T2^*$	654	625	620	644	621	618
2						
N^*	544	562	479	542	545	472
T^*	—	629	—	—	617	—
$T1^*$	592	—	580	590	—	578
$T2^*$	647	—	608	643	—	606
3						
N^*	552	528	495	549	522	491
$T1^*$	607	601	597	606	600	596
$T2^*$	658	648	621	658	643	619

from the maximum expected value of 0.4 due in part to non-coincidence of the absorption and emission transition dipole orientations but mainly due to partial rotational diffusion depolarization in *n*-octanol during the excited state lifetime (ca. 4 ns, see below). The emission anisotropy also shows a sharp change in value coincident with the two emission bands. When excited at 320 nm all values are negative and there is a small but neat difference in the absolute value, greater for the N^* band than for the T^* band. This observation confirms that N^* and T^* emission transition dipoles do not coincide but make a small angle between them.

The time resolved emission of **1**–**3** shows decay curves that can be very well fitted to the typical sum of two exponential terms expected for the dynamics of the ESIPT process (see figure 5). The decay curves and TRES correspond to the so called thermodynamic behavior of ESIPT, i.e. a fast equilibration of the N^*–T^* transformation in the excited state, prior to a much slower decay of the excited state equilibrated mixture. This conclusion is supported by: (i) the faster time is 10 to >100 times shorter than the slower one; (ii) in the red band of the emission spectrum, where T^* is responsible for the emission, the faster component has a negative amplitude; (iii) TRES shows a fast decrease of the relative contribution of N^* at the beginning of the decay, while the relation of N^* to T^* emission remains constant after the first ns of the decay; (iv) area normalized TRES show an isoemissive point, typical of systems with two interconvertible emitting species. In this kinetic regime, the faster time component is assigned to the ESIPT equilibrium, and is therefore given by the sum of the rate constants for the forward and backward tautomerization steps, whereas the longer time component is a weighted average of the decay rates of N^* and T^*.

A remarkable difference between compounds **1**–**3** and 3-HC derivatives substituted only on ring B is that the T^* emission, though relatively increasing with time, is present in a high proportion already at the beginning of the decay. The conclusion is that the *N*–*T* equilibrium also exists in the ground state, with the two species overlapping in their absorption band such that both are excited by the photolysing pulse at 405 nm. The presence of ESIPT was inferred because the N^*/T^* concentration ratio initially excited and the equilibrium ratio in the excited state are different. In all cases the excited state equilibrium contains a higher proportion of *T* than the mixture immediately after excitation at 405 nm.

For **1** and **3**, but not for **2**, the contribution of N^* to the total emission prior to equilibration is negligible. As a consequence, for **1** and **3**, the equilibrated excited state emission spectrum is indistinguishable from the steady state spectrum, a consequence of the very fast equilibration time of the tautomerization in the excited state (on the order of 10 ps for **1** and **3**, compared to N^* or T^* deactivation rates, ~3 ns, for the same compounds). As can be deduced from TRES in compound **1** (see figure 6), the initially excited composition (405 nm excitation) contains ~3 times more N^* than the equilibrium in the excited state.

Table 2 summarizes the fitted lifetimes of the decays for the three compounds at different temperatures and in different solvents. Compound **2** showed a much slower equilibration, corresponding to k_{fast}, than the other compounds. Remarkably, the slower component, k_{slow}, shows a lifetime increase as the temperature raises. This behavior is a consequence of the ESIPT equilibrium displacement with temperature as will be discussed later.

DFT calculations of the three compounds were performed in the *N* and *T* geometry. Computed dipole moments in DCM in the ground *N* and *T* states as well as in the excited N^* and T^* states (table 3) indicate a great polarity increase in the probes after excitation, which would explain the positive solvatochromism and the blue thermochromic shift upon temperature increase. The HOMO-LUMO electronic transition of these compounds shows the typical charge transfer character, reflected in the charge density shift from one part of the molecule to practically the complementary part in the *N* conformation (figure 7). This shift is greater for the molecules studied in this work than for the parent compounds reported in the literature with a substituent only in ring B (DMAHF and FHC), because the present compounds have the possibility of delocalizing charge on the substituent on ring A, absent in the other compounds. In the supporting information we include details of calculated charges on selected atoms and moieties. Compound **2** has the greatest dipole moment increase upon excitation of the three species, which explains its greatest Stokes

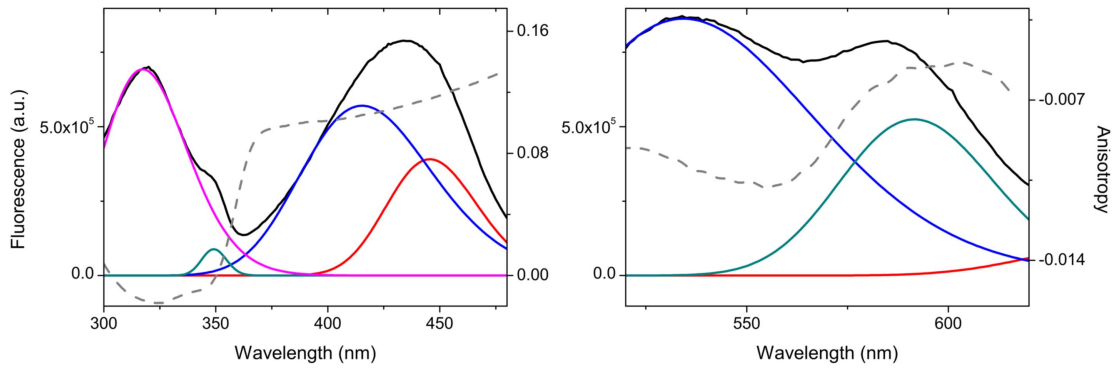

Figure 4. Steady state anisotropy of **3** (gray dashed curve in both panels) in *n*-octanol at 15 °C. For both panels, the curve in black represents the total corrected steady state spectrum. The Gaussian components of the deconvolution are shown. Left panel: excitation anisotropy. $\lambda_{em} = 530$ nm. Right panel: emission anisotropy. $\lambda_{exc} = 320$ nm.

shift in the series. In a solvent, and as a consequence of the mutual polarizability of probe and solvent molecules, the dipole moment increase will be surely larger. Figure 6 also shows the orientation of the transition dipole moments for the two lowest absorption bands for the two tautomers of compound **2**. The calculations support the evidence from the fluorescence polarization spectra for the two absorption transitions between 300 and 500 nm with perpendicular transition moments.

4. Discussion

We will make several references of the features of ring A substituted compounds **1**–**3** as compared to parent compounds DMAHF and FHC, as well as to 7-aryl-3-HC. Compared to DMAHF, compound **1** has an electron donor substituent on ring A, while **3** has an electron acceptor. Compared to FHC, compound **2** has an electron donor acceptor on ring A, besides the difference between a furyl moiety (FHC) replaced by a thiophene moiety (**2**).

The push–pull feature of compounds **2** and **3** is reflected in their greater dipole moment increase upon excitation, as compared to compound **1** (see table 3). More interesting is the fact that in push–pull compounds **2** and **3**, the presence of an electron acceptor group on ring B and an electron donor on ring A has much more effect on the dipole moment increase in the excited state (**2**) than when the type of substituents is exchanged (**3**). This is evidenced by the higher dipole moment increase in **2** upon excitation (16 D) compared to **3** (9.2 D), as reflected by calculations, and the larger Stokes shift of **2** in DCM at 25 °C (7140 cm^{-1}, N^* emission maximum) compared to 4400 cm^{-1} for **3** under the same conditions. This is also in line with the higher solvatochromic susceptibility of a 7-(4-dimethylamino)phenyl-3-HC compared to DMAHF [20]. The HOMO and LUMO charge distribution (see figure 7) supports the smaller polarity change of T upon excitation as compared to N, as reported in the literature, which is reflected in the smaller solvatochromic shift of the T emission band when compared to the N emission.

We also studied the temperature dependence of the emission energy of both tautomers and the behavior of the relative emission of N^* and T^*. For compound **2**, that displays the largest effects and the more extreme kinetic behavior, the study was extended to a broader temperature range. In all cases, the thermochromic behavior is consistent with a higher interaction of the excited state than the ground state with the solvent. This feature leads to a blue shift of the emission energy with temperature increase. Consistently with the solvatochromic behavior, the thermochromic shift is greater for **2** than for **1** and **3**, and in all three compounds, the energy shift in the emission is greater for N^* than for T^*.

The emission ratio of N^* to the total emission: $I_{N^*}/(I_{N^*} + I_{T^*})$, see figure 3, remains constant with temperature change for **1** and it decreases for both **2** and **3**. The behavior of **1** is similar to that of its parent compound DMAHF [36]. In the referenced paper, the authors explain the behavior by the fast establishment of an equilibrium between N^* and T^*, which is maintained during the excited state decay. To observe a temperature independent emission ratio of N^* and T^*, the position of the equilibrium and the ratio of the emission quantum yields of the compounds must be temperature independent. Nevertheless, **3**, and to a greater extent, **2**, show a decrease of the fraction of N^* emission upon increasing the temperature. Near room temperature, the three compounds behave like the system described: essentially a decay of N^* and T^* in equilibrium. The different tendency of $I_{N^*}/(I_{N^*} + I_{T^*})$ with temperature is a consequence of the equilibrium shift with temperature in the excited state. Moreover, for **2**, this equilibrium shift is accompanied by an increase in the lifetime decay corresponding to the slower time component around and above room temperature (see table 2). Both of these effects can be rationalized if we assume that temperature increase shifts the excited state equilibrium of the tautomers to

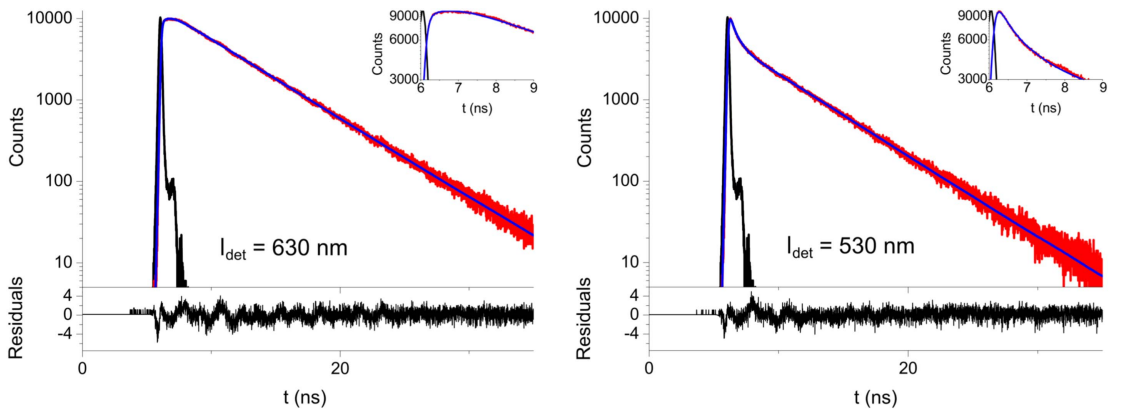

Figure 5. Emission time profiles (red curve) with instrument response function (black curve), biexponential fit (blue curve) and residuals for **2** in DCM at 20 °C. Samples were excited at 405 nm and emission was detected at 630 (left panel) and at 530 nm (right panel). The insets show the detail of the fast component of the decay. The parameters of the fit are: for 630 nm, A1 = −0.011; $\tau 1 = 0.54 \pm 0.06$ ns; A2 = 0.037; $\tau 2 = 4.46 \pm 0.02$ ns; for 530 nm, A1 = 0.024; $\tau 1 = 0.47 \pm 0.02$ ns; A2 = 0.014; $\tau 2 = 4.31 \pm 0.03$ ns.

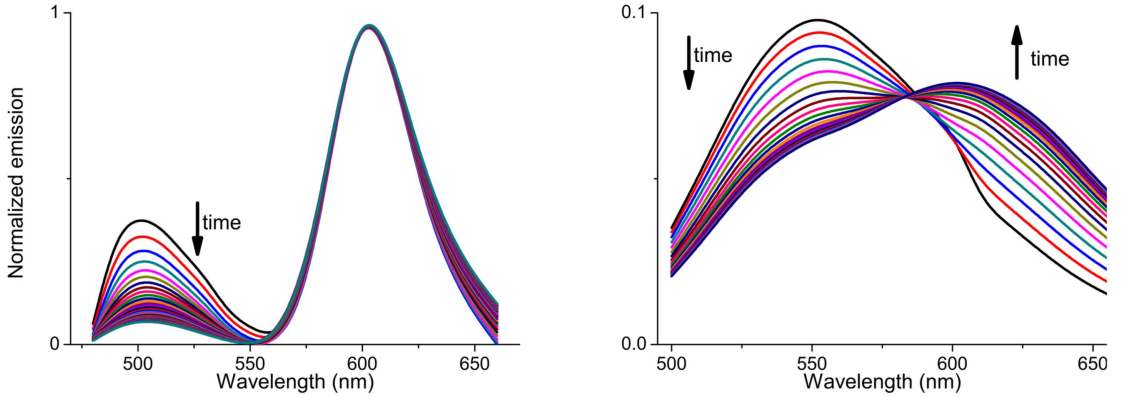

Figure 6. Time resolved emission spectra in DCM at 25 °C. Spectra were reconstructed from decay curves registered at 10 nm intervals in the plotted range for each compound. Left panel: compound **1**. Spectra are normalized to the maximum. Spectra are displayed at 10 ps intervals in the range 0–1 ns. Right panel: compound **2**. Area normalized spectra. Spectra are displayed at 100 ps intervals in the range 0–2 ns.

a mixture that is enriched in T^*. This means that the N^*–T^* transformation is endothermic in the excited state (as it is in the ground state) [16]. This equilibrium shift directly explains the greater proportion of T^* emission with temperature raise. To explain the life-time increase, we will analyze in detail the kinetics of the excited state reaction and decay as follows.

The ESIPT process is explained by the kinetic equations derived from reaction scheme 2 [7].

$$\frac{d[N^*]}{dt} = -(k_{NT} + k_N) \,.\, [N^*] + k_{TN} \,.\, [T^*], \quad (1)$$

$$\frac{d[T^*]}{dt} = k_{NT} \,.\, [N^*] - (k_{TN} + k_T) \,.\, [T^*]. \quad (2)$$

Equations (1) and (2) lead to the well-known sum of two exponential terms for the time dependence of N^* and T^* with two characteristic times. The expression of these two time constants ($k_{fast} = 1/\tau_{fast}$; and $k_{slow} = 1/\tau_{slow}$) can be derived from the solution of the differential equations. They can be more compactly expressed in a general way by their sum and product as:

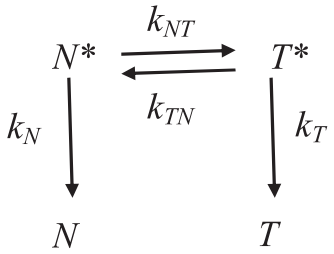

Scheme 2. Reaction mechanism for the ESIPT process and excited state decay.

$$k_{fast} + k_{slow} = k_{NT} + k_{TN} + k_N + k_T, \quad (3)$$

$$k_{fast} \,.\, k_{slow} = k_{NT} \,.\, k_T + k_N \,.\, (k_{TN} + k_T). \quad (4)$$

If the equilibration steps are much faster than the decay, i.e. k_{NT}, $k_{TN} \gg k_N$, k_T; then the faster and the slower time constants assume the form:

$$k_{fast} = k_{NT} + k_{TN}, \quad (5)$$

Table 2. Lifetimes of the biexponential decay of emission for **1–3** in different solvents at different temperatures. The values are averages from decays recorded at different emission wavelengths, as given in each case, after 405 nm excitation.

Compound	Solvent	T(K)	τ_{fast} (ns)	τ_{slow} (ns)
1	ACN 480–660 nm	298	<0.005	3.03
	DCM 480–660 nm	288	0.010	3.03
		318	0.007	2.38
	Tol 475 and 600 nm	288	0.016	3.00
		318	<0.005	2.65
2	DCM 530 and 630 nm	198	2.63	3.90
		228	1.60	3.91
		248	1.12	3.93
		288	0.544	4.01
		298	0.459	4.19
		308	0.388	4.34
		318	0.321	4.45
		328	0.283	4.53
	Tol 465 and 580 nm	288	0.155	4.08
		318	0.354	3.96
3	DCM 520 and 600 nm	288	<0.005	2.68
		318	<0.005	2.19
	Tol 485 and 600 nm	288	0.032	2.87
		318	0.010	2.28

$$k_{slow} = k_T \cdot \frac{k_{NT}}{k_{NT} + k_{TN}} + k_N \cdot \frac{k_{TN}}{k_{NT} + k_{TN}}. \quad (6)$$

Equations (5) and (6) show the well-known result that the fast time constant corresponds to the equilibration of the tautomerization step, whereas the slow time constant is an average of the N^* and T^* decay rate, weighted by the fraction of each species present at equilibrium. In the general case, i.e. when the two time constants are comparable, the expression for the individual k_{fast} and k_{slow} is each a quadratic form including both the four reaction rates. Using equations (5) and (6), we can explain the qualitative aspects of the kinetic behavior of **1–3** with temperature. Both k_{NT} and k_{TN} can be activated processes, being their respective activation energies $E_{NT} > E_{TN}$ for an endothermic tautomerization. The slow constant can decrease with temperature if $k_T < k_N$ and the fraction of T^* increases with temperature increase, as a consequence of the endothermic tautomerization. For **1** and **3** (see table 2), as $k_{fast} > 30 \times k_{slow}$, the two processes: equilibration and decay, are well separated. For **2**, above 280 K $k_{fast} > 5 \times k_{slow}$, reaching a factor of 8 at the highest temperature measured, as a consequence of an opposite variation with temperature of k_{fast}, that raises with temperature, and k_{slow}, that decreases with temperature. Below 280 K the two global rate constants become quite similar and the approximations used to derive equations (5) and (6) are not valid. Therefore, to fit the data the complete solution must be used. To this aim, equations (3) and (4) are easier to handle than the complex explicit expressions for each lifetime, derived from them without any approximation. Therefore, to fit the data for compound **2**, we used the sum and the product of the observed rates, as depicted by equations (3) and (4). At high temperature, the process with the highest activation energy should prevail, this would be k_{NT}. Consequently we derived the Arrhenius parameters for this rate constant for **2** from the high temperature data of k_{fast}. These values are: $A_{NT} = 450\ ns^{-1}$; $E_{NT} = 13.7\ kJ\ mol^{-1}$, for the pre exponential factor and the activation energy of k_{NT}, respectively. On the other side, we considered that the high temperature behavior of k_{fast} reflects the excited state lifetime of T^*, and therefore, $k_T = 0.22\ ns^{-1}$. Once we fixed these values, we fitted the whole rate constant set of k_{fast} and k_{slow} of compound **2** to the expressions of equations (3) and (4) to obtain $A_{TN} = 13.4\ ns^{-1}$, $E_{TN} = 10\ kJ\ mol^{-1}$, and $k_N = 0.25\ ns^{-1}$. The values of these parameters were able to reproduce faithfully the experimental behavior of the decay rate constants of **2** in a temperature range from −80 °C to 55 °C in DCM, as shown in figure 8 (see also SI). Considering the values of the activation energy for the forward and the backward tautomerization in the excited state, E_{NT} and E_{TN}, we conclude that T^* is ca. 4 kJ mol^{-1} higher in energy than N^*. This value, as well as the values of the activation energies, in the order of 10 kJ mol^{-1} for these rate constants, is in agreement with what was measured and calculated for DMAHF in acetonitrile and in DCM [13, 15]. The equilibrium constant in the excited state between N^* and T^* can be calculated from ratio of the forward and backward rate constants of the transformation: $\boldsymbol{K^*_{NT}} = [T^*]/[N^*] = k_{NT}/k_{TN} = 34.\exp(-3.7\ kJ/mol/RT)$.

The comparison of **2** with the kinetic behavior of FHC shows some differences. FHC in non protic solvents has a tautomerization lifetime that rises from <15 ps in acetonitrile to 200 ps in formamide [37]. At 298 K, **2** displays a lifetime of 460 ps for its faster component in DCM. Moreover, FHC is characterized as an example of irreversible proton transfer in the excited state, due to its kinetic behavior, and thus it is deduced that T^* is much lower in energy than N^*. In **2** this situation is inverted, as the kinetic results show (N^* to T^* transition is endothermic). This can be explained by the stabilization of N^* caused by the energy donating moiety in ring A.

5. Conclusions

We studied the spectroscopic and kinetic features as a function of temperature of three 3-HC substituted in rings A and B with moieties that display different electron donor–acceptor characteristics. They show a similar solvatochromic and thermochromic tendency as 3-HC compounds substituted only in ring B but, the push–pull compounds **2** and **3** display a greater thermochromic sensitivity and a greater change with temperature of the emission intensity ratio between N^* and T^*. Calculations demonstrate the greater charge delocalization upon electronic excitation, which is enabled by the presence of the substituent on ring A.

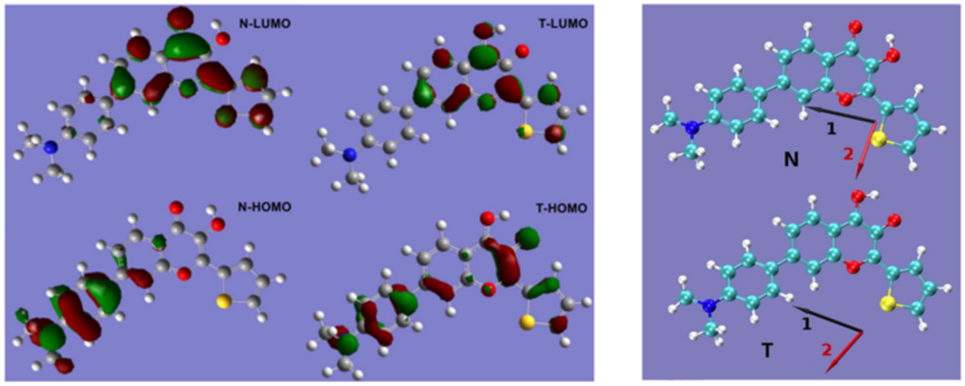

Figure 7. Left panel: molecular orbitals of isodensity of 0.04 e bohr^{-3} are displayed for the HOMO and LUMO of the *N* and *T* forms of compound **2**. Right panel: Ground state geometry of *N* and *T* forms of compound **2**. The arrows show the orientation of the transition dipole moments for the HOMO-LUMO (1) and the HOMO-LUMO +1 (2) transitions for each tautomer.

Table 3. Dipole moments (in Debye units) of *N* and *T*, ground states, and N^* and T^*, excited states, for **1–3**.

1				2				3			
N	N^*	*T*	T^*	*N*	N^*	*T*	T^*	*N*	N^*	*T*	T^*
9.4	14.4	10.6	10.7	8.4	24.4	10.8	12.2	7.6	16.8	7.4	8.1

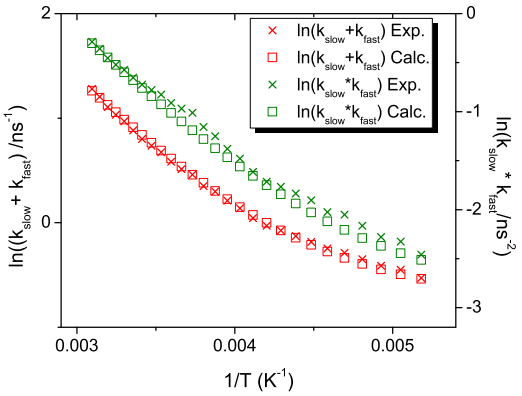

Figure 8. Arrhenius type plots for the sum and the product of the two time constants of the decay of **2** in DCM. The experimental values represented as crosses are taken from table 2. The squares are calculated values using the kinetic parameters of the text.

The excited state kinetics can be well explained by a reversible and comparatively fast tautomerization equilibration in the excited state, followed by decay of the equilibrated tautomer ratio. Especially for **2**, the kinetics is very particular and sensitive to temperature changes. The push–pull substitution pattern in the two rings enhances environment and temperature sensitivity of these ESIPT ratiometric fluorescent probes.

Acknowledgments

LG, VMS, and PFA are Research Staff and AS is a Research Fellow from CONICET (Consejo Nacional de Investigaciones Científicas y Técnicas, Argentina). This work was performed under financial support from grant PICT 2013-1931 from ANPCyT (Ministerio de Ciencia, Tecnología e Innovación Productiva, MinCyT, Argentina). The funders had no role in study design, data collection and analysis, decision to publish, or preparation of the manuscript. We used TUPAC Cluster from CSC-CONICET, which is part of SNCAD-MinCyT, Argentina. We thank Dr Raphael da Silva Alvim (ABCsim-UFABC) for resources and advice and Dr Thomas Jovin (Max-Planck Institute for Biophysical Chemistry, Göttingen, Germany) for critically reading the manuscript. The authors have declared that no competing interests exist.

References

[1] Klymchenko A S and Demchenko A 2003 Multiparametric probing of intermolecular interactions with fluorescent dye exhibiting excited state intramolecular proton transfer *Phys. Chem. Chem. Phys.* **5** 461–8

[2] Zhao J, Ji S, Chen Y, Guo H and Yang P 2012 Excited state intramolecular proton transfer (ESIPT): from principal photophysics to the development of new chromophores and applications in fluorescent molecular probes and luminescent materials *Phys. Chem. Chem. Phys.* **14** 8803–17

[3] Yushchenko D A, Fauerbach J A, Thirunavukkuarasu S, Jares-Erijman E A and Jovin T M 2010 Fluorescent ratiometric MFC probe sensitive to early stages of alpha-synuclein aggregation *J. Am. Chem. Soc.* **132** 7860–1

[4] Shynkar V V, Klymchenko A S, Kunzelmann C, Duportail G, Muller C D, Demchenko A P, Freyssinet J M and Mely Y 2007 Fluorescent biomembrane probe for ratiometric detection of apoptosis *J. Am. Chem. Soc.* **129** 2187–93

[5] Kwon J E and Park S Y 2011 Advanced organic optoelectronic materials: harnessing excited-state intramolecular proton transfer (ESIPT) *Process. Adv. Mater.* **23** 3615–42

[6] Sengupta P K and Kasha M 1979 Excited state proton-transfer spectroscopy of 3-hytdroxyflavone and quercetin *Chem. Phys. Lett.* **68** 382–5
[7] Tomin V I, Demchenko A P and Chou P-T 2015 Thermodynamic versus kinetic control of excited-state proton transfer reactions *J. Photochem. Photobiol.* C **22** 1–18
[8] Demchenko A P, Tang K C and Chou P-T 2013 Excited-state proton coupled charge transfer modulated by molecular structure and media polarization *Chem. Soc. Rev.* **42** 1379–408
[9] Schwartz B J, Peteanu L A and Harris C B 1992 Direct observation of fast proton transfer: femtosecond photophysics of 3-hydroxyflavone *J. Phys. Chem.* **96** 3591–8
[10] Tomin V I, Oncul S, Smolarczyk G and Demchenko A P 2007 Dynamic quenching as a simple test for the mechanism of excited-state reaction *Chem. Phys.* **342** 126–34
[11] Ghosh D, Batuta S, Das S, Begum N A and Mandal D 2015 Proton transfer dynamics of 4′-N,N-dimethylamino-3-hydroxyflavone observed in hydrogen-bonding solvents and aqueous micelles *J. Phys. Chem.* B **119** 5650−61
[12] Dereka B, Letrun R, Svechkarev D, Rosspeintner A and Vauthey E 2015 Excited-state dynamics of 3-hydroxyflavone anion in alcohols *J. Phys. Chem.* B **119** 2434−43
[13] Roshal A D, Organero J A and Douhal A 2003 Tuning the mechanism of proton-transfer in a hydroxyflavone derivative *Chem. Phys. Lett.* **379** 53–9
[14] Shynkar V V, Mély Y, Duportail G, Piémont E, Klymchenko A S and Demchenko A P 2003 Picosecond time-resolved fluorescence studies are consistent with reversible excited-state intramolecular proton transfer in 4′-(Dialkylamino)-3-hydroxyflavones *J. Phys. Chem.* A **107** 9522–9
[15] Zhang W, Shia B and Shi J 2005 Time-dependent density functional investigation on electronic spectra of 4′-N-dimethylamino-3-hydroxyflavone *J. Mol. Struct.: THEOCHEM* **731** 219–24
[16] Kenfack C A, Klymchenko A S, Duportail G, Burger A and Mély Y 2012 *Ab initio* study of the solvent H-bonding effect on ESIPT reaction and electronic transitions of 3-hydroxychromone derivatives *Phys. Chem. Chem. Phys.* **14** 8910–8
[17] Klymchenko A S, Pivovarenko V G, Ozturk T and Demchenko A P 2003 Modulation of the solvent-dependent dual emission in 3-hydroxychromones by substituents *New J. Chem.* **27** 1336–43
[18] Strandjord A J G and Barbara P F 1985 The proton-transfer kinetics of 3-hydroxyflavone: solvent effects *J. Phys. Chem.* **89** 2355–61
[19] Chou P-T, Pu S-C, Cheng Y-M, Yu W-S, Yu Y-C, Hung F-T and Hu W-P 2005 Femtosecond dynamics on excited-state proton/charge-transfer reaction in 4′-N,N-diethylamino-3-hydroxyflavone the role of dipolar vectors in constructing a rational mechanism *J. Phys. Chem.* A **109** 3777−87
[20] Giordano L, Shvadchak V V, Fauerbach J A, Jares-Erijman E A and Jovin T M 2012 Highly solvatochromic 7-Aryl-3-hydroxychromones *J. Phys. Chem. Lett.* **3** 1011−16
[21] M'Baye G, Klymchenko A S, Yushchenko D A, Shvadchak V V, Ozturk T, Mely Y and Duportail G 2007 Fluorescent dyes undergoing intramolecular proton transfer with improved sensitivity to surface charge in lipid bilayers *Photochem. Photobiol. Sci.* **6** 71−6
[22] Klymchenko A S and Mély Y 2004 7-(2-Methoxycarbonylvinyl)-3-hydroxychromones: new dyes with red shifted dual emission *Tetrahedron Lett.* **45** 8391–4
[23] Klymchenko A S, Yushchenko D A and Mely Y 2007 Tuning excited state intramolecular proton transfer in 3-hydroxyflavone derivative by reaction of its isothiocyanate group with an amine *J. Photochem. Photobiol.* A **192** 93−7
[24] Giordano L, Shvadchak V V, Fauerbach J A, Jares-Erijman E A and Jovin T M Environment-sensitive fluorophore based on 2-aryl-7-aryl-3-hydroxychromone (to be published)
[25] Ehrhardt C, McQuire L W, Rigollier P, Rogel O, Shultz M and Tommasi R A 2009 *Arylsulfonamide-Based Matrix Metalloprotease Inhibitor* PCT Int. Appl.WO2009118292(A1) 136pp https://register.epo.org/espacenet/regviewer?AP=09724483&CY=EP&LG=en&DB=REG
[26] Klymchenko A S and Mely Y 2004 7-(2-Methoxycarbonylvinyl)-3-hydroxychromones: new dyes with red shifted dual emission *Tetrahedron Lett.* **45** 8391–4
[27] Frisch M J *et al* 2009 Gaussian 09, Revision B01, (Wallingford CT: Gaussian, Inc.) http://gaussian.com/g09_b01
[28] Yanai T, Tew D P and Handy N C 2004 A new hybrid exchange–correlation functional using the Coulomb-attenuating method (CAM-B3LYP) *Chem. Phys. Lett.* **393** 51–7
[29] Adamo C and Jacquemin D 2013 The calculations of excited-state properties with time-dependent density functional theory *Chem. Soc. Rev.* **42** 845–56
[30] Tomasi J and Persico M 1994 Molecular interactions in solution: an overview of methods based on continuous distributions of the solvent *Chem. Rev.* **94** 2027−94
[31] Barone V, Cossi M and Tomasi J 1997 A new definition of cavities for the computation of solvation free energies by the polarizable continuum model *J. Chem. Phys.* **107** 3210−21
[32] Improta R, Barone V, Scalmani G and Frisch M J 2006 A state-specific polarizable continuum model time dependent density functional theory method for excited state calculations in solution *J. Chem. Phys.* **125** 054103
[33] Gunduz S, Goren A C and Ozturk T 2012 Facile syntheses of 3-hydroxyflavones *Org. Lett.* **14** 1576–9
[34] Cortés J, Heitele H and Jortner J J 1994 Band-shape analysis of the charge-transfer fluorescence in barrelene-based electron donor-acceptor compounds *J. Phys. Chem.* **98** 2527–36
[35] Tseng H-W, Shen J-Y, Kuo T-Y, Tu T-S, Chen Y-A, Demchenko A P and Chou P-T 2016 Excited-state intramolecular proton-transfer reaction demonstrating anti-Kasha behavior *Chem. Sci.* **7** 655–65
[36] Oncul S and Demchenko A P 2006 The effects of thermal quenching on the excited-state intramolecular proton transfer reaction in 3-hydroxyflavones *Spectrochim. Acta* A **65** 179–83
[37] Das R, Klymchenko A S, Duportail G and Mély Y 2009 Unusually slow proton transfer dynamics of a 3-hydroxychromone dye in protic solvents *Photochem. Photobiol. Sci.* **8** 1583–9